Three-dimensional seismic ground motion modeling in inelastic basins Jifeng Xu¹, Jacobo Bielak², Omar Ghattas², and Jianlin Wang³

Abstract

In this paper we report on the development and application of a parallel numerical methodology for simulating large-scale earthquake-induced ground motion in highly heterogeneous basins whose soil constituents can deform nonlinearly. We target sedimentary basins with large contrasts in wavelengths for which regular grid methods become inefficient, and overcome the problem of multiple physical scales by using unstructured finite element triangulations. We illustrate the methodology with an example of an idealized basin, which contains a deep and a shallow sub-basin. The simulations show significant amplitude reduction of the ground accelerations due to inelastic soil behavior at sites above the deepest portions of the sub-basins, yet little shift in frequency. Under the assumption of linear anelastic material behavior, there is a rapid spatial distribution of the ground acceleration of the basin, which differs markedly from that for a one-dimensional analysis. This characteristic three-dimensional nature of the ground motion is preserved for the elastoplastic model. Concerning the ground displacement, the main qualitative difference between the elastic and inelastic models is the occurrence of significant permanent deformations in the inelastic case. These residual displacements can have practical implications for the design of long structures such as bridges and structures with large plan dimensions.

Introduction

Nearly all the models used until recently in seismology for predicting ground motion induced by earthquakes have been based on the assumption of linear elastic behavior of the soil. On the other hand, for a number of years nonlinear soil amplification has been routinely taken into consideration in geotechnical engineering practice (Seed and Idriss, 1969; Finn, 1991). The main reason seismologists had in the past ignored the possibility that nonlinear phenomena could play an important role in earthquake ground motion was that compelling evidence for nonlinear effects in the observed motion, other than in liquefied sites, was scarce. In the last decade, however, a number of accelerograms have been recorded during strong earthquakes that have made it possible to infer nonlinear response. The most common manifestations of inelastic soil behavior involve the reduction in shear wave velocity and the increase in soil damping with increasing load (Hardin and Drnevich, 1972). Accordingly, the corresponding nonlinear site effects include the lowering of the site amplification factor as the amplitude of the seismic loading increases; in some cases this is accompanied by the lowering of the resonance frequencies in the spectra of the recorded ground. Thus,

¹ The Boeing Company, P. O. Box 3707 MC 7L-21, Seattle, WA 98124-2207, jifeng.xu@boeing.com

² Department of Civil and Environmental Engineering, Carnegie Mellon University, Pittsburgh, PA 15213, jbielak@cs.cmu.edu; oghattas@cs.cmu.edu

³ Synopsis, Inc. 700 East Middlefield Rd., Mountain View, CA 94043, jianlin@synopsis.com

evidence of nonlinear soil response during strong earthquakes can be identified directly if weak and strong motion records are simultaneously obtained on the ground surface and at depth in a borehole, or through simulation, as long as records are available for strong shaking. As these simultaneous records have been rare, nonlinear site effects is oftentimes inferred from ground motion records obtained during strong and weak earthquakes at both rock and soil locations by filtering out the earthquake source radiation and propagation path effects. Identifying an appropriate reference rock site, though essential for this approach, still represents a considerable challenge, as rock properties at the free surface differ from those at the basement.

Nonlinear soil behavior has received increased attention from seismologists in recent years. SMART1 (Strong Motion Accelerograph Array in Taiwan) and SMART2 (Abrahamson et al, 1987) have provided reliable records of events available for the study of nonlinear site effects in a particular seismic region in Taiwan in which a carefully established downhole accelerograph array was deployed. Analyses of these record (Chang et al., 1989; Wen et al., 1994; Beresnev et al, 1995) revealed significant nonlinear soil response in both deamplification and degradation of wave velocities in ground motions with peak ground acceleration larger than 0.15g. In Japan, nonlinear behavior of soil sediments was identified at Kuno in the Ashigara valley by using borehole records (Satoh et al, 1995). At Port Island, the motion at different depths recorded during the 1995 Hyogoken-Nambu by a borehole array demonstrated strong nonlinear features of seismic amplification in reclaimed land areas and also in Holocene and Pleistocene soil deposits (Sato et al, 1996). The Loma Prieta earthquake of 1989 in California presents another case in which nonlinear site effects have been detected. Chin and Aki (1991) found a pervasive nonlinear site effect at sediment sites in the epicentral region by eliminating the influences of the radiation pattern and topography. They concluded that the site amplification factor depends on the acceleration level and nonlinear effect may appear at levels above 0.1g to 0.3g. This is in the range expected from geotechnical engineering studies. Darragh and Shakal (1991) estimated the response of a soil site by studying the ratio of the smoothed Fourier amplitude spectra from a soil site and a nearby rock site, and observed pronounced strong motion deamplification effects. The 1994 Northridge earthquake also presents plausible evidence of nonlinear soil response. Trifunac and Todorovska (1996) estimated an upper bound on the distance from the earthquake source where nonlinear soil response affects peak acceleration. They analyzed the observed strong motion amplitudes in the San Fernando valley and found that noticeable reduction in recorded horizontal peak accelerations occur at sites with shear wave velocity less than 360 m/s and distance from the fault less than 15-20 km. By comparing ground-motion between the Northridge earthquake and its aftershocks, Field et al (1997) reported that sediment deamplification was up to a factor of two during the main shock implying significant nonlinearity. More recently, O'Connell (1999) has shown that much of the same data can be explained by linear response and scattering of waves in the upper kilometers of the earth's crust. Strong motion deamplification effects were also observed for the aftershocks of the 1983 Coalinga earthquake in California by Jarpe et al (1988)

Besides the well-known amplitude deamplification and changes in resonance frequency, Archuleta (1998) has identified a characteristic spiky waveform in some strong motion accelerograms as evidence of nonlinear response. Archuleta et al (2000) cite a number of examples where this spiky waveform has been observed. This characteristic high frequency waveform was first noticed by Porcella (1980) and later thoroughly analyzed by Iai et al (1995).

Simulations of nonlinear earthquake response began in the late 1960s. These early studies were conducted for horizontally layered soils and vertically incident waves, by either an equivalent linear or a direct nonlinear method. These are the main methods that are still used today in engineering practice. In the equivalent linear method, the soil response is evaluated in an iterative manner. First, trial values for average strain are chosen, then soil properties are determined in accordance with the trial values of strain, and finally the response of the model is calculated. If the calculated strains differ significantly from the trial values, the cycle is repeated (Seed and Idriss, 1968; Schnabel et al, 1972). Many studies have concluded that equivalent linear approach cannot reproduce some of the important characteristics of the seismic ground motion, especially for the cases of strong loadings (Streeter et al, 1974; Finn et al, 1978). The equivalent linear method overestimates the seismic response due to pseudo-resonance at periods corresponding to the strain-compatible stiffness used in the final elastic iteration analysis. Also, since the method is elastic it cannot predict the permanent deformations that occur during an earthquake.

In the direct nonlinear method, the shear modulus is modified at every time step according to the current strain, so that the nonlinear stress-strain relationship is closely followed. A number of representations have been used for the backbone curves and yield rules of soil stress-strain relationships. They include, e.g., linear (Idriss and Seed, 1968), multilinear (Joyner and Chen, 1975; Yu et al, 1993), and one by Archuleta et al (2000) based on a modified Masing rule with a provision for pore pressure (Elgamal, 1991).

While one-dimensional (1D) simulations can yield reasonable estimates of nonlinear effects under vertically incident seismic excitation, they cannot represent the effects of surface waves and basin effects. The few 2D and 2.5D studies to date of nonlinear soil amplification (e.g., Joyner and Chan, 1975; Joyner, 1975; Elgamal, 1991; Marsh et al, 1995; Zhang and Papageorgiou, 1996) have confirmed the importance of nonlinearity on site response. In particular, a 2.5D study of the Marina District in San Francisco during the 1989 Loma Prieta earthquake found that the focusing and lateral interferences often observed in studies based

on linear soil behavior are still present for strong excitation though not as prominently as for weak excitation (Zhang and Papageorgiou, 1996). The use of an equivalent linearization technique meant that no permanent deformations could be detected.

In this study we describe a finite element methodology for modeling three-dimensional ground motion in basins, including inelastic behavior of the soil, due to arbitrary seismic excitation, and illustrate it for an idealized basin. The soil within the basin is idealized as a Drucker-Prager elastoplastic material (Drucker and Prager, 1952). Results show that whereas the ground motion decreases due to soil nonlinearity, the spatial variation of this motion follows closely that of the linear model, showing clear basin effects. Also, despite the significant reduction in peak response, there is only a small change in the dominant frequencies.

Method of Analysis

The mathematical problem under consideration is one of earthquake-induced waves traveling from a flat-layered halfspace of rock into a basin with heterogeneous and possibly nonlinear soils and irregular geometry. We assume small deformations throughout. We will use standard finite element techniques to solve this problem. Topics of special importance in the development of the model, such as the governing equations, the constitutive laws governing the materials, the type of loading, and the type of elements are discussed briefly next; details can be found in Xu (1998).

The governing equation for the balance of momentum is given by:

$$\rho \ddot{\mathbf{u}} - \nabla \cdot \boldsymbol{\sigma} = \mathbf{f} \tag{0.1}$$

where ρ is the density of the material, **u** is the displacement vector field, $\boldsymbol{\sigma}$ is the stress tensor field, and **f** is the body force, which as will be explained subsequently, is introduced to represent the seismic excitation.

Standard Galerkin discretization in space by finite elements produces a system of ordinary differential equations of the form:

$$\mathbf{M} \ddot{\mathbf{U}}(t) + \sum_{e} \int_{V^e} \mathbf{B}^T \boldsymbol{\sigma} \, dV^e = \mathbf{F}(t)$$
 (0.2)

where \mathbf{M} is the global mass matrix; \mathbf{U} is the nodal displacement time-dependent vector; \mathbf{F} is a time-dependent vector of applied nodal forces; V^e is the element volume; \mathbf{B} is the element matrix of shape function derivatives; and $\boldsymbol{\sigma}$ is the current stress tensor within each element computed by an appropriate procedure from the soil constitutive law. This system of equations is nonlinear because the stress $\boldsymbol{\sigma}$ depends nonlinearly on the current displacement \mathbf{U} and the loading history.

The main factor influencing the reliability of numerical calculations of nonlinear dynamic soil behavior is the implementation of the stress-strain law. For this initial analysis of the ground motion of soil deposits in 3D basins we idealize the soil, both clays and sands, as a Drucker-Prager material. We selected this material because: (1) the implementation of its constitutive law is similar to that required for more complex constitutive laws; (2) it can represent soil dilatancy and its parameters can be related to the physical soil properties (cohesion and friction angle) in a rather straightforward way; and (3) despite its relative simplicity, it can lead to reasonable agreement between the results of simulations and observations for problems that do not involve soil liquefaction. This satisfactory performance of the Drucker-Prager model was observed, in particular, in a study aimed at predicting the monotonic and cyclic response of pile foundations to axial and lateral loads (Trochanis et al, 1991).

In our implementation of the finite element method we use lumped mass diagonal matrices for each element, and the integral in the second term in (2) is evaluated by Gauss numerical integration. As is usually done in displacement-based finite element formulations, the algorithmic framework for the elastoplastic analysis is strain driven. Given a prescribed strain increment at a step n + 1, the problem is to update the stress tensor at each Gauss point at the new time t_{n+1} given its value at the previous time t_n . We use a return mapping algorithm (Ortiz et al, 1983; Simo and Taylor, 1986), which is capable of accommodating arbitrary yield criteria, flow rules, and hardening laws.

In order to treat efficiently large-scale 3D problems that involve elastoplastic laws, we use an element-by-element procedure to implement equation (2) into our software. That is, the product of the mass matrix and the corresponding nodal accelerations, and the second term in (2) are evaluated separately for each finite element and then assembled. Notice that no global matrices need to be stored; only vectors need to be assembled.

We have built a parallel elastoplastic wave propagation simulation code on top of Archimedes, an environment for solving unstructured mesh finite element problems on parallel computers ("Archimedes", 1988), as a generalization of our earlier parallel elastic wave propagation simulation code (Bao et al, 1998). Archimedes includes 2D and 3D mesh generators, a mesh partitioner, a parceler and a parallel code generator. We favor finite elements for their ability to efficiently resolve multiscale phenomena by tailoring the mesh size to local wavelengths, and the ease with which they handle traction interface and boundary conditions, and complex geometries, including arbitrary topography. Since the mesh generator in Archimedes builds meshes that are made up of tetrahedra with straight edges, we use 10-node subparametric quadratic tetrahedral for our calculations. The reason we introduce a quadratic approximation of the displacement field within each element, rather than the linear approximation we used for our elastic models, is to be able to represent exactly linear

strain fields, for as it is well-known, piecewise constant strain approximation lead to poor accuracy for elastoplastic problems.

Two important issues must be considered for solving wave propagation problems in infinite domains by the finite element method. One is the need to render the domain of computation finite and to limit the occurrence of spurious reflections. This is accomplished here by introducing an absorbing boundary condition at the outer boundary of the computational domain. We use a simple dashpot approach (Lysmer and Kuhlemeyer, 1969) for this purpose, which consists of adding viscous dampers at each boundary node. This gives rise to a diagonal damping matrix with non-zero terms associated only with boundary nodes.

The second point that requires attention is the need to incorporate the seismic excitation into the model, which for the example we will consider later consists of an incident plane wave. This is carried out by means of a two-step method developed by Bielak and his co-workers (Bielak and Christiano, 1984; Cremonini et al, 1988; Bielak et al, 2001). In the first step, one introduces an auxiliary model that encompasses the source and a background structure from which the basin has been removed. The second problem models the local site effects. Its input is a set of equivalent localized forces derived from the first step. These forces act only within a single layer of elements adjacent to the interface between the exterior region and the region of interest.

Model Verification

Before we can apply the incremental finite element code just described to a general situation, it is necessary to verify it against known solutions from established methods. To check the purely linear version of our new software we compared results for simple idealized situations (Bao, 1998) against those from our linear wave propagation software tool (Bao et al, 1998), with satisfactory results.

Nonlinear analysis of 3D problems presents some difficulties to both developers and users of finite element technology. Unlike linear problems, in a model undergoing inelastic deformation, both normal and shear components of stress undergo changes corresponding to changes of either the normal or shear component of strain. It is well known that finite element plasticity solutions can become highly inaccurate, especially in the fully plastic range. Inaccuracies occur not only due to numerical inaccuracies but also due to the basic incremental character of the plasticity law. To verify the correctness of our implementation and test the accuracy of our numerical procedure, we developed several small-scale test problems (Xu, 1998) and compared the results with those from ABAQUS (from Hibbit, Karlsson, and Sorensen, Inc. Providence, Rhode Island), a well-tested commercial software package.

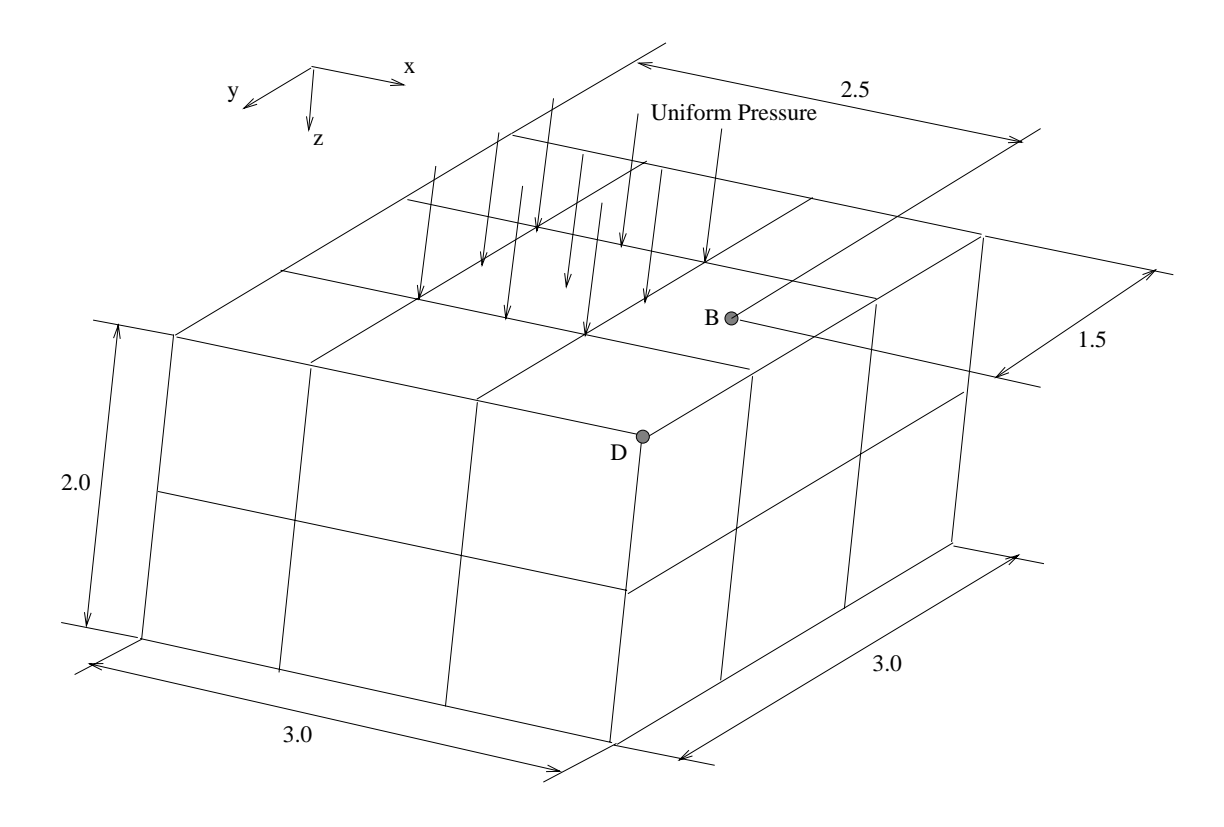
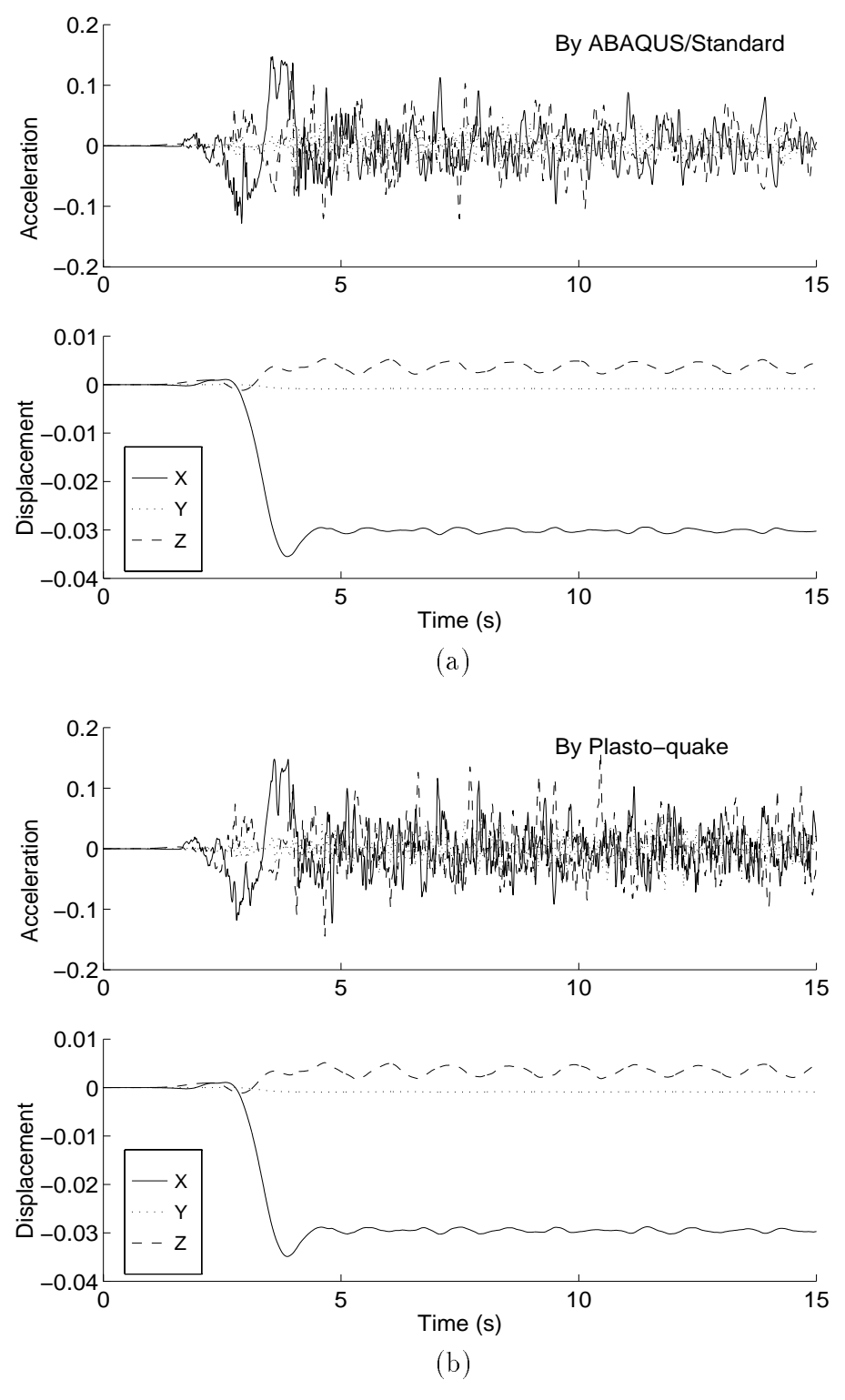


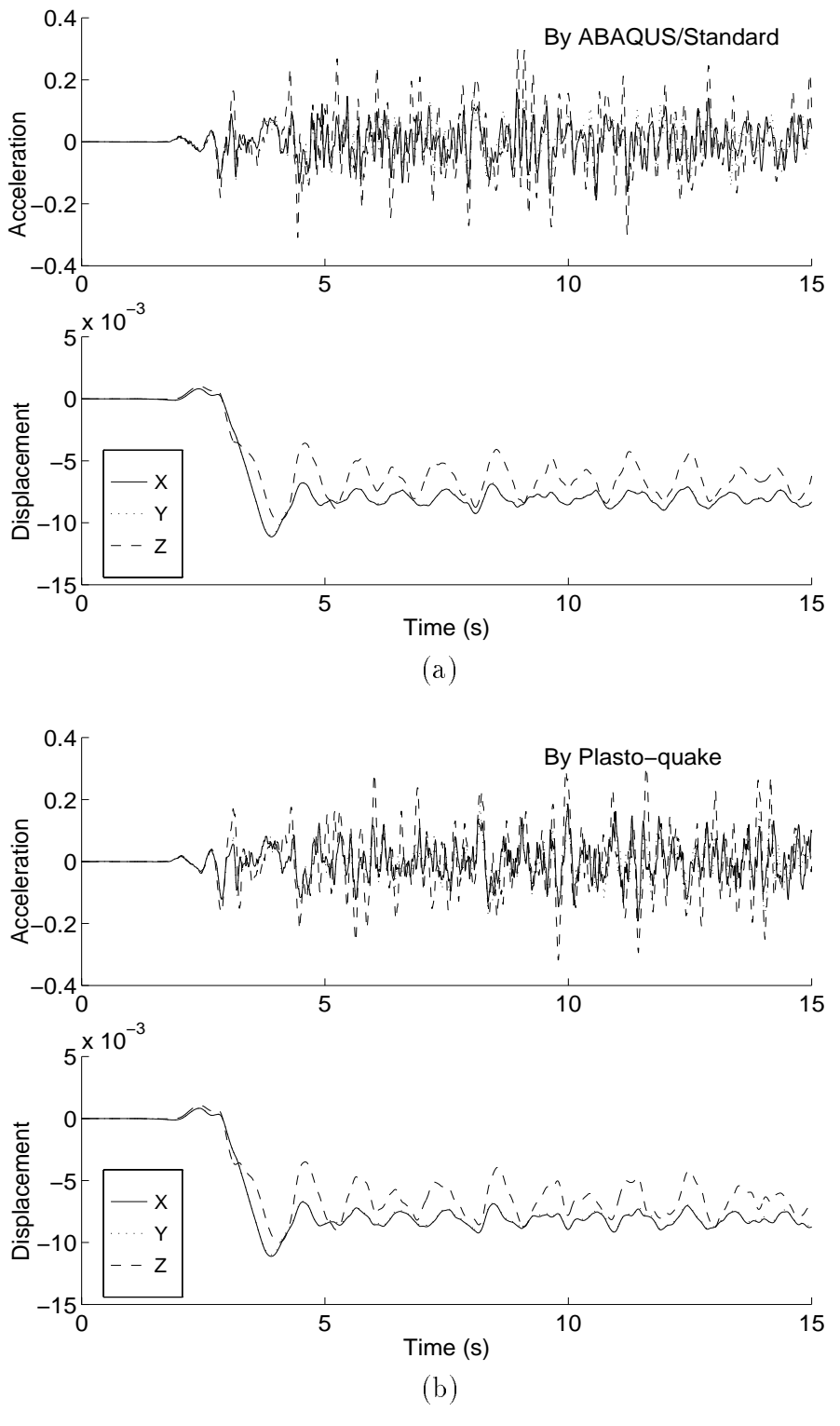
Figure 1: Test problem for elastoplastic computations with a quadratic tetrahedral mesh. The cube is subjected to a uniform distributed load on the central portion of its top surface that varies like a Ricker pulse over time.

We present here results from one of these tests. The physical problem under study is a solid cube fixed at the bottom surface and subjected to a uniform pressure over a central portion of its top surface, as shown in Figure 1. The remaining sides are traction-free. The material is modeled by an elasto-perfectly-plastic Drucker-Prager law (with zero frictional angle). The applied pressure varies in time as a Ricker pulse with a central frequency of 0.4Hz. The cube is divided into smaller cubes and each cube is, in turn, subdivided into tetrahedra with straight edges. Nodes are assigned at each vertex and midside, and the solution for the displacement field within each tetrahedron is of the form of a complete quadratic polynomial. This results in the 10-node subparametric quadratic tetrahedral element mentioned earlier. We use an explicit central difference method to solve the equations of motion (2) and four-point Gauss numerical quadrature to evaluate the integral in the second term.

Synthetic acceleration and displacement seismograms obtained by our code are shown in Figures 2 and 3 for two locations, B and D on the top surface of the cube. These are labeled Plasto-quake, after our code's name. The corresponding results obtained with ABAQUS using the exact same elements are also shown in these figures, for comparison. Instead of



 $\label{eq:Figure 2: Comparison of dynamic response at B by: (a) ABAQUS/Standard with implicit method; (b) Plasto-quake with explicit method. Displacements and accelerations are shown in the direction of the three coordinate axes.}$



 $\label{eq:Figure 3: Comparison of dynamic response at D by: (a) ABAQUS/Standard with implicit method; (b) Plasto-quake with explicit method. Displacements and accelerations are shown in the direction of the three coordinate axes.}$

an explicit solver, ABAQUS uses an implicit solver in conjunction with the 10-node tetrahedron. Even though our explicit solver requires a smaller time step, which is dictated by the Courant stability criterion, it can be parallelized readily. The agreement between the results of the solutions is very good, both for accelerations and displacements. Notice that whereas the displacement seismograms are fairly smooth, the accelerograms exhibit spikes (high frequency components) analogous to those described by Archuleta et al (2000). Some of these may correspond to the actual solution; others correspond to noise from our numerical approximations, as we expect our model to provide accurate solutions only for frequencies up to 1.0Hz, corresponding to the rule of 10 points per wavelength we used to construct the finite element mesh. One measure of the numerical error is given by the traces for the displacement in the y-direction at point B, which should be identically zero due to symmetry (part of the error arises, of course because the mesh is not completely symmetric about the vertical plane through B).

Illustrative Example

We now examine the effects of 3D nonlinear soil behavior on seismic ground motion of an idealized heterogeneous basin with an irregular basement. The basin, shown in Figure 4, consists of a 100m soil layer underlain by a stiffer soil of variable depth, which are surrounded by an elastic halfspace. The basin has a maximum depth of 1km and a length of 4km. The label I refers to the box that defines the boundary of the computational domain, where the absorbing boundary conditions are applied. The effective earthquake excitation is applied on the strip of elements between II and III, which is the next to the outermost layer of elements. Five points on the basin's surface, A, B, C, D, and E, are used to describe the basin response. The material in the basin is taken to be stiff Lower Oxford unweathered clay and is assumed to obey the Drucker-Prager elastoplastic constitutive relations. The corresponding cohesion and friction angle are given in Table 1. This table also lists the density, elastic and attenuation properties of the soil deposits and surrounding halfspace. These properties are assumed to remain constant over time, i.e., no degradation is taken into consideration. The anelastic attenuation is taken to be of the Rayleigh type, i.e., within each finite element the damping matrix is assumed to be a linear combination of the mass and initial tangent stiffness matrices. This yields a damping ratio, 1/(2Q(w)), that is inversely and directly proportional to frequency, respectively. The factors of proportionality are selected so as to minimize the integral of the squared difference between the actual frequency-varying damping ratio and the target damping ratio, 1/(2Q) (Bielak et al, 1999).

The excitation consists of a transient, vertically incident SV-wave polarized in the direction of the x-axis (axis of symmetry through line ABCD). The forcing function is a Ricker pulse with a central frequency of 0.28Hz, and the surface free-field peak acceleration outside the

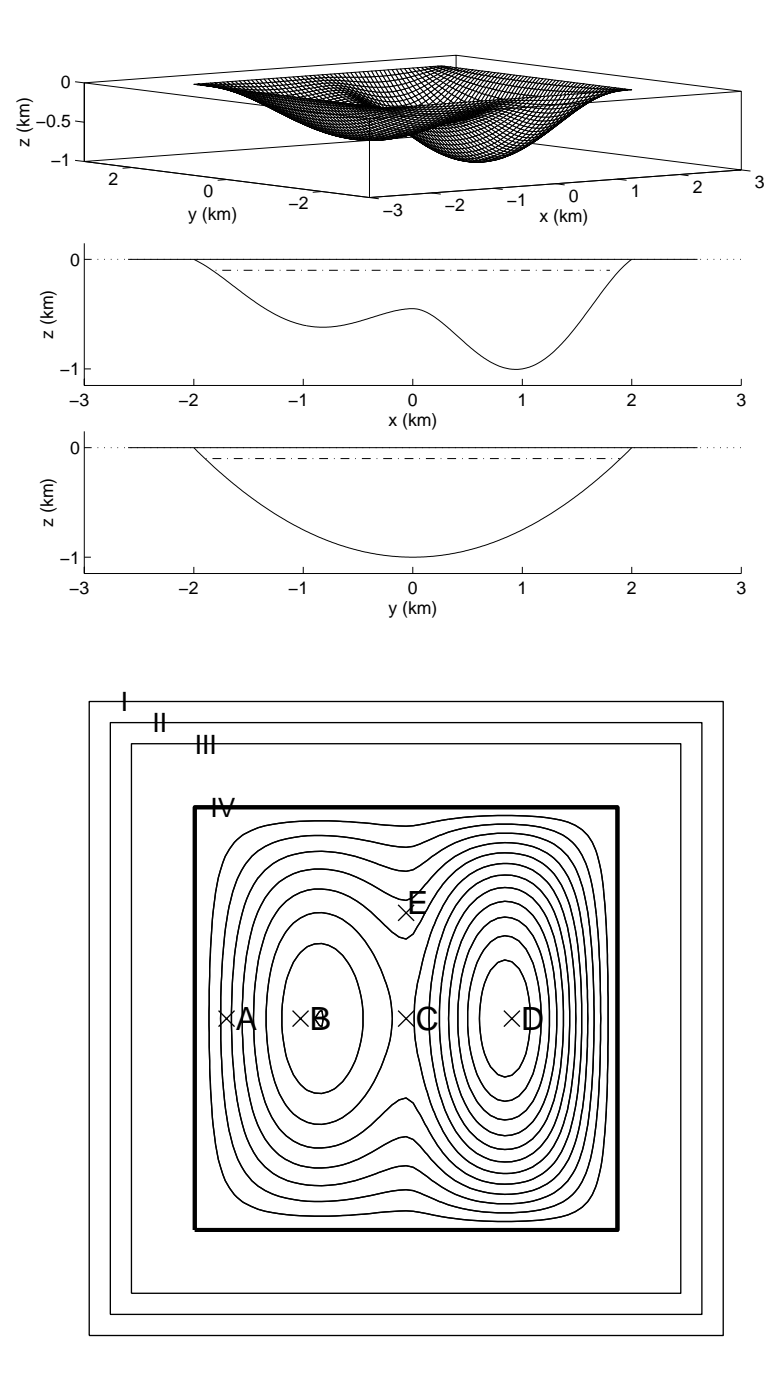


Figure 4: Idealized three-dimensional basin, surrounded by an elastic halfspace. (a) Interface between basin and rock and cross-sections through plane of symmetry and deepest portion of largest sub-basin; (b) Plan view of basin with contour lines of basement surface. Each step is 77m. A, B, C, D, and E are observation points, and I, II, III, and IV are various surfaces described in the text.

	Density	Poisson's	Shear Wave	Attenuation	Cohesion	Friction
		Ratio	${f Velocity}$	Factor		Angle
	(g/cm^3)		(m/s)		(kPa)	(°)
Top	1.85	0.32	200	25	55	17
Second	1.90	0.30	400	50	160	20
Halfspace	2.10	0.28	800	100	-	-

 $Table\ 1:\ Material\ properties\ of\ basin\ layers\ and\ the\ surrounding\ halfspace.\ Layers\ obey\ Drucker-Prager\ elastoplastic\ constitutive\ law;\ halfspace\ is\ linearly\ elastic.\ In\ addition,\ all\ three\ materials\ have\ attenuation.$

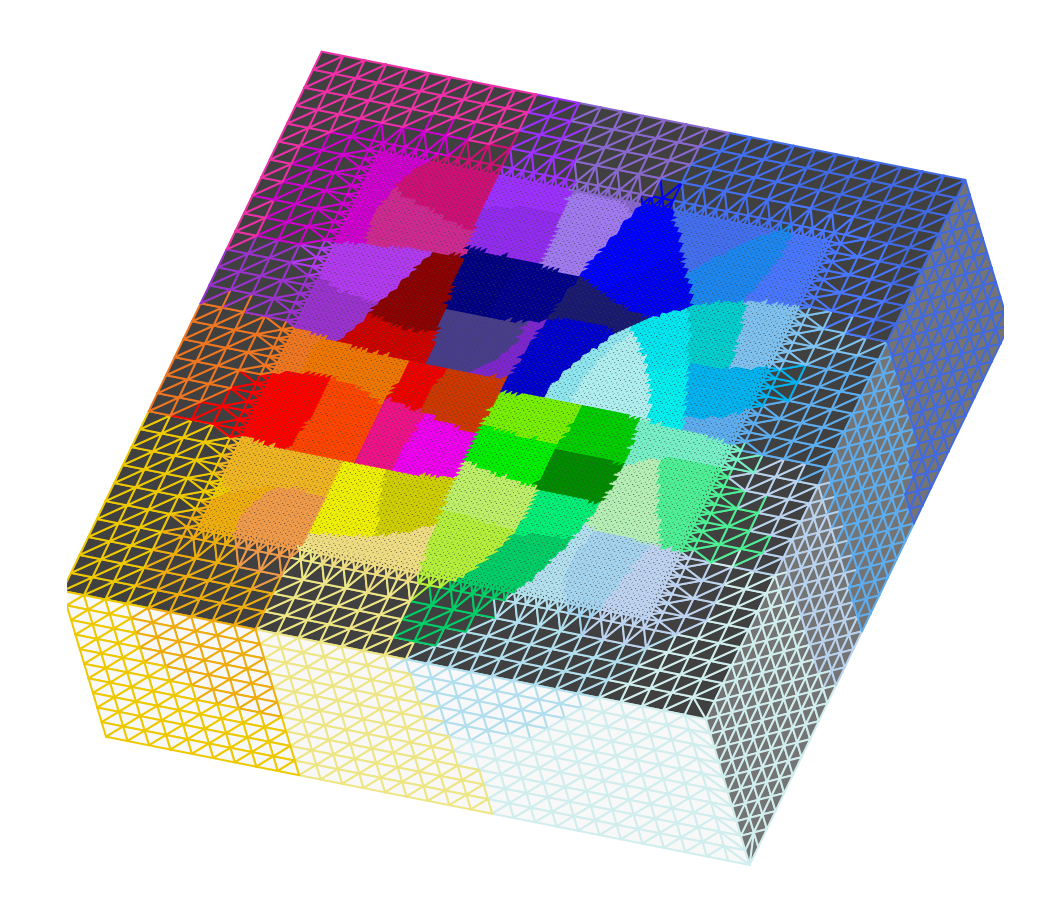


Figure 5: Finite element mesh partitioned for 64 subdomains.

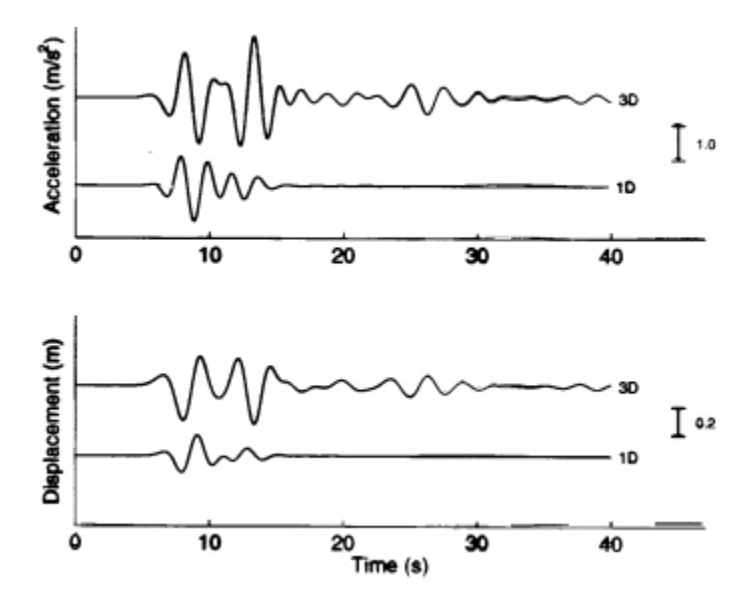


Figure 6: Acceleration and displacement seismograms at Point D from 1D simulation and 3D simulation, in the direction of the x-axis.

basin is 0.06g. With the material properties and excitation frequencies established, the finite element mesh is tailored to the local wavelengths. The shortest wavelength at a given point is determined by the local shear wave velocity and the highest frequency of the input excitation, which is taken to be 0.8Hz. For future reference, the first resonant frequency of the top layer under linear elastic behavior is 0.5Hz. The resulting mesh, coarsened for visualization purposes and partitioned into 64 subdomains, is shown in Figure 5. It has on the order of 280,000 elements, 400,000 nodes, and, thus, close to one million degrees of freedom. The simulations were executed on 128 processors of the Cray T3D at the Pittsburgh Supercomputing Center.

While the main objective of the present analysis is to examine basic differences between the (an)elastic response and inelastic response of the basin, we are also interested in assessing the basin effects on the ground motion; that is, we ask the question of how different is the 3D response of the basin from that for a one-dimensional (1D) analysis. For this comparison we concentrate only on the elastic response and consider a single free-surface location, D, above the deepest part of the basin. The 1D analysis was performed for a soil column whose properties are identical to those beneath point D, using as input the same incident SV-wave as for the 3D simulation. The main effects of the lateral confinement of the basin on ground motion are illustrated by Figure 6, which shows the horizontal components of acceleration and displacement at D in the direction of motion x of the incoming wave. The seismograms have been low-pass filtered to 0.8Hz, in keeping with the accuracy of our numerical approximations. Here and in the subsequent figures we focus on the horizontal ground motion because, except for ground settlement, this is the one that controls the

earthquake performance of constructed facilities. In agreement with previous investigations (e.g., Bielak et al, 1999, Olsen, 2000), the basin affects the 1D response in two important ways. First, it significantly increases the maximum amplitude of the response, and second, it extends the duration of the strong phase of the ground motion. For instance, whereas the peak 1D acceleration is 0.10g, the corresponding 3D value is 0.18g; also, the duration of shaking is more than double for 3D than for 1D. This comparison shows that neglecting 3D effects can lead to erroneous results. Accordingly, all subsequent results refer to our 3D model.

Given the peak acceleration of 0.18g we expect that the soil will exhibit nonlinear behavior. Figure 7 shows the horizontal acceleration and displacements in the x-direction at the five locations shown at the bottom of Figure 5. Results are presented both for an elastic model in which the yielding of the soil material is not allowed, and for the elastoplastic case. The accelerograms have been low-pass filtered to 0.8Hz in keeping with the accuracy of our numerical approximations. This removes spikes such as those present in Figures 2 and 3, analogous to those reported by Archuleta et al (2000) from actual records. For the elastic model, the amplification of the incoming wave is very strong atop the deepest points above the two sub-domains, with a peak value of about 3, and surface Rayleigh waves are prominent. Surface waves are also responsible for the much longer duration of the ground motion within the basin than in the free field and with respect to that for the 1D analysis. The convex shape of the basement in the middle region precludes the amplification of the amplitude of motion and longer duration from developing at C, where a defocusing effect, in contrast to the focusing that takes place at B and D, is clearly visible.

The main effect of the elastoplastic soil behavior on the accelerations shown in Figure 7 is to reduce the amplitude of the maximum response, by about a factor of 2 in the deepest regions where the shear strains are largest. Closer to the basin edge this effect is smaller; the reduction at A is only ten percent. It is noteworthy that contrary to many 1D soil amplification studies, no significant reduction is observed in the dominant frequencies of the response and that the surface wave effects remain quite strong for the elastoplastic case. A comparison of displacement synthetics shows that the main qualitative difference with the elastic simulation of displacements is the occurrence of permanent deformations. The distribution of these horizontal and vertical residual displacements within the basin is shown in Figure 8. Permanent vertical displacements are responsible for structure settlements, as observed in Mexico City during the 1985 Michoacan earthquake. Further, differential ground displacement is responsible for damage to long structures and structures with large plan dimensions. It is interesting that while the horizontal permanent displacement varies gradually over the basin and the peaks occur in the regions of maximum depth, the displacement in the vertical direction, exhibits a rapid spatial variation, and the peak values

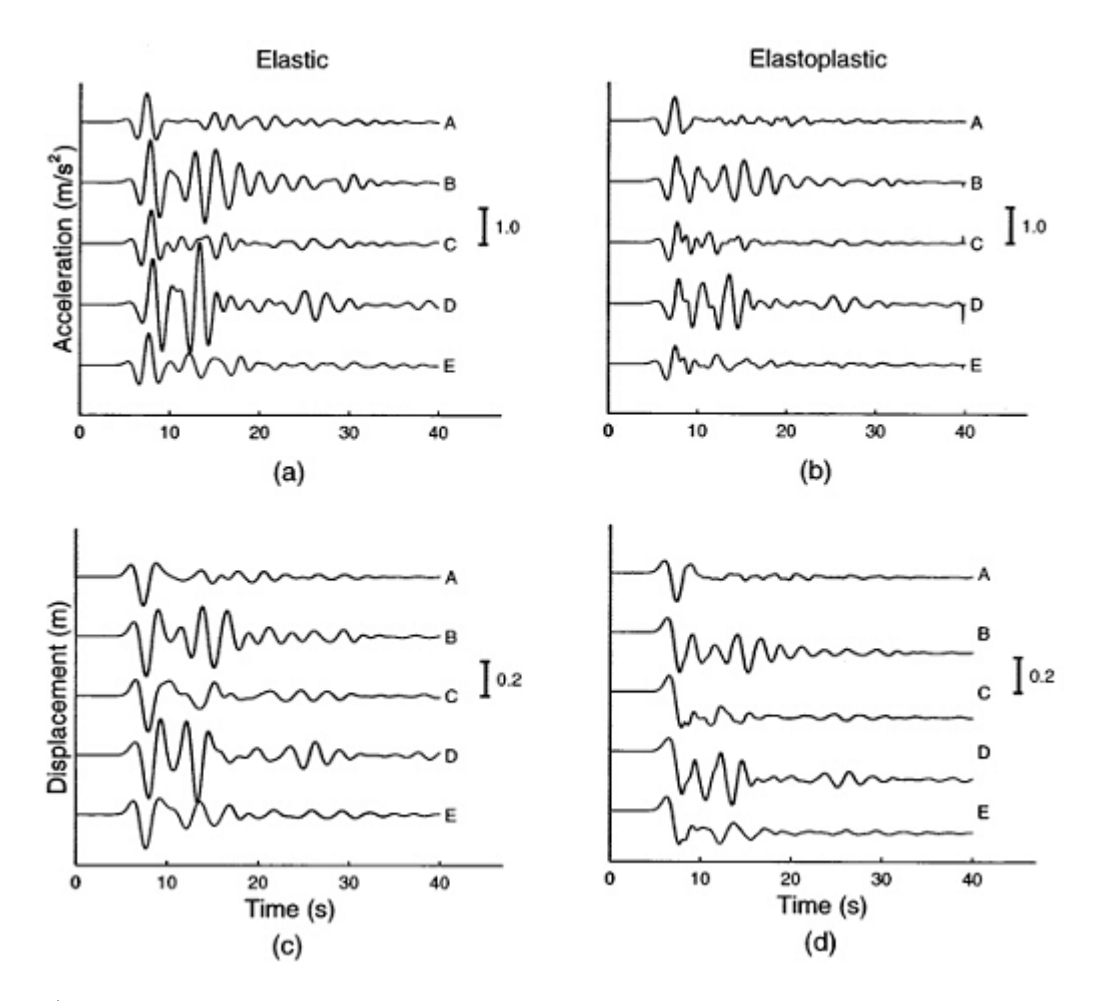


Figure 7: Elastic and elastoplastic displacement and acceleration seismograms in the x-direction at the observation points shown in Figure 4.

occur near the basin confluences.

It is usual in engineering applications to use a single parameter to estimate the severity of an earthquake at a particular location. Peak acceleration is perhaps the most common one. This value, however, is not a good predictor of potential damage to most engineering structures, as it is related to the response of structures with very high frequencies, and represents a value that may occur only at an isolated instant. In the following, we use instead another quantity, the acceleration Arias intensity (Arias, 1970), which provides an average value of the ground acceleration over the entire duration of the seismic event. This quantity is defined as the tensor quantity:

$$I_{ij} = \frac{\pi}{2g} \int_0^T a_i(t)a_j(t)dt \tag{0.3}$$

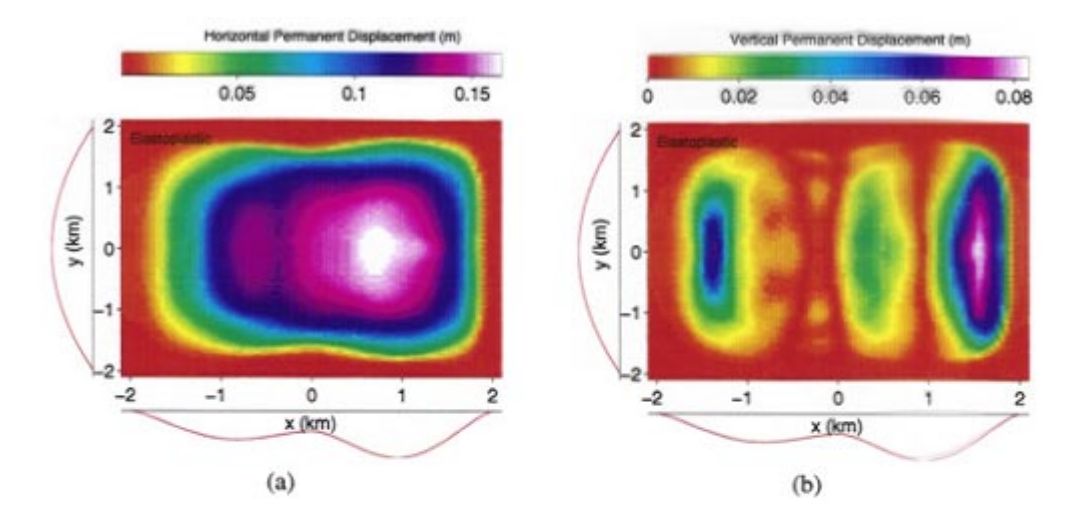


Figure 8: Residual displacements within the basin. (a) Horizontal along x-axis; (b) Vertical.

where T is the earthquake duration, and $a_i(t)$ is the component of ground motion acceleration in the *i*th direction. The total horizontal Arias intensity is defined as:

$$I_h = I_{xx} + I_{yy} \tag{0.4}$$

The square root of I_h is shown in Figure 9 for the elastic and elastoplastic cases, respectively. We use the square root so that the plotted quantity will vary linearly with the peak free-field acceleration in the elastic case. Reflecting the difference in the accelerograms, the peak value of the intensity for the elastoplastic case is about one half that for the elastic case. The spatial distribution of the two, however, is similar, with maxima occurring above the deepest points. The Arias intensity varies considerably (up to a factor of 2.5 for the elastic case and 2 for the elastoplastic one) away from the edges. The three-dimensionality of the response is apparent, as different points underlain by essentially the same soil layers exhibit different responses. Naturally, a 1D analysis would predict identical results at points with the same soil characteristics.

To further examine the basin effects on the ground motion, another parameter introduced by Arias (1996) to measure the dominant orientation of the horizontal ground motion is plotted in Figure 10. This parameter, denoted by δ , is defined by:

$$\delta = \frac{\left[\left(I_{xx} - I_{yy} \right)^2 + 4I_{xy}^2 \right]^{1/2}}{I_{xx} + I_{yy}} = \frac{I_1 - I_2}{I_1 + I_2} \tag{0.5}$$

in which I_1 and I_2 are the largest and smallest principal horizontal Arias acceleration intensities. δ varies between zero and one. If $\delta = 0$, the ground motions in the x and y directions are comparable. On the other hand, if $\delta = 1$, the horizontal motion occurs only

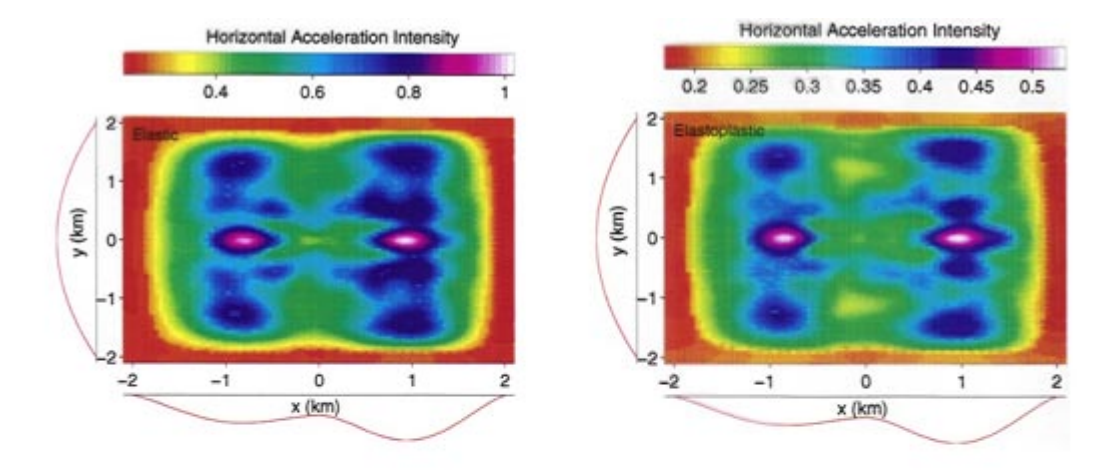


Figure 9: Distribution of Arias acceleration intensity, $(Ih)^{1/2}$, within the basin surface, in $(m/s)^{1/2}$. Left panel: elastic model; Right panel: elastoplastic model. Notice different scales, but pattern similarity.

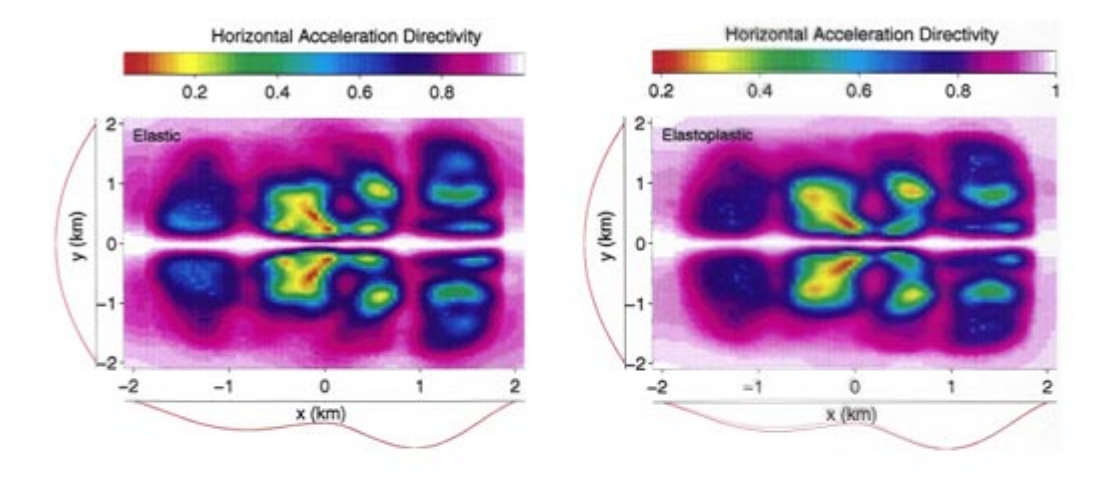


Figure 10: Distribution of Arias acceleration directivity, within the basin surface. This parameter is a measure of the variability of the dominant orientation of horizontal ground acceleration throughout the basin. $\delta=1$ indicates motion only along x-axis; $\delta=0$ denotes comparable motion in the x- and y-directions. Left panel: elastic model; Right panel: elastoplastic model.

in a single direction. Clearly, on the axis of symmetry, which contains the points ABDE, the ground motion takes place along that axis, since the incident wave is polarized along the x-axis. Despite the simple nature of the incident motion, the ground motion shows a variety of dominant orientations, as characterized by the wide range of δ . Since for a 1D analysis δ would be equal to unity throughout the basin, the variability of this parameter underscores the significance of the basin effects on ground motion. Notice that for this idealized basin the directivity coefficient for the elastoplastic case exhibits essentially the same pattern as for the elastic case.

Concluding remarks

In summary, results of our simulations show that the elastoplastic soil behavior results in an overall reduction of the ground acceleration throughout the basin. On the other hand, the characteristic 3D spatial distribution of the ground acceleration observed for the elastic basin is also preserved in the elastoplastic case. This means that one-dimensional analyses usually performed to evaluate nonlinear effects might need to be re-evaluated to account for basin effects. In addition, in our nonlinear example the soils experienced significant residual displacements; these cannot be modeled by linear or equivalent nonlinear analyses. The presence of nonlinearity in ground motion is good news in that the amplifying effects of sediments, on average, are apparently not as great as implied by weak-motion studies. On the negative side, lack of linearity suggests that methods such as the empirical Green's function method that make use of recordings of small earthquakes to predict strong ground motion at sediment sites might have to be revised to take nonlinearity of the surficial soils into consideration. Also, spatial dynamic displacements and residual deformations can have practical implications for the design and retrofit of long structures, such as bridges and structures with large plan dimensions.

Acknowledgment

This work was supported by the National Science Foundation's High Performance Computing and Communication program and KDI program, under grants CMS-9318163 and CMS-9980063. The cognizant program director is Dr. Clifford J. Astill. Computing services on the Pittsburgh Supercomputing Center's Cray T3D were provided under PSC Grant BCS-960001P. We are grateful for this support. Thanks also to Antonio Fernández for help with the preparation of the figures.

References

- Abrahamson, N. A., Bolt, B. A., Darragh, R. B., Penzien, J., and Tsai, Y. B. (1987). "The SMART1 accelerograph array (1980 1987), a review." *Earthquake Spectra*, 3, 263–287.
- Archimedes (1998). "Archimedes." (www.cs.cmu.edu/~quake/Archimedes.html).
- Archuleta, R. J., Bonilla, L. F., and Lavallee, D. (2000). "Nonlinearity in observed and computed accelerograms." In *Paper No. 1934, Proc. 12th World Conf. on Earthquake Eng.*, Auckland, New Zealand.
- Archuleta, R. J. (1998). "Direct observation of nonlinear soil response in acceleration time histories." Seism. Res. Lett., 69, 149.
- Arias, A. (1970). "A measure of earthquake intensity." In Hansen, R. J., editor, Seismic Design for Nuclear Power Plants, pages 438–483, MIT Press, Cambridage, Massachusetts.
- Bao, H., Bielak, J., Ghattas, O., Kallivokas, L. F., O'Hallaron, D. R., Shewchuk, J. R., and Xu, J. (1998). "Large-scale Simulation of Elastic Wave Propagation in Heterogeneous Media on Parallel Computers." Computer Methods in Applied Mechanics and Engineering, 152(1-2), 85-102, January.
- Bao, H. (1998). "Finite element simulation of earthquake ground motion in realistic basin." *Ph.D Thesis*, Carnegie Mellon University, Pittsburgh, PA.
- Beresnev, I. A., Wen, K. L., and Yeh, Y. T. (1995). "Seismological evidence for nonlinear elastic ground behavior during large earthquakes." Soil Dyn. Earthquake Eng., 14, 103–114.
- Bielak, J. and Christiano, P. (1984). "On the effective seismic input for nonlinear soil-structure interaction systems." *Earthquake Engrg. and Struct. Dyn.*, 12, 107–119.
- Bielak, J., Xu, J., and Ghattas, O. (1999). "On earthquake ground motion and structural response in alluvial valleys." J. Geotech. and Geoenv. Eng., 125, 413–423.
- Bielak, J., Loukakis, K., Hisada, Y., and Yoshimura, C. (2001). "Domain reduction method for three-dimensional earthquake modeling in localized regions. Part I: Theory." *Bull. Seism. Soc. Am.*, submmitted. (www.andrew.cmu.edu/~jbielak/DRM_PART1.pdf).
- Chang, C. Y., Power, M. S., Tang, Y. K., and Mok, C. M. (1989). "Evidence of nonlinear soil response during a moderate earthquake." In *Proc. 12th Int. Conf. on Soil Mechanics and Foundation Engineering*, volume 3, pages 1–4, Rio de Janeiro.

- Chin, B. H. and Aki, K. (1991). "Simultaneous study of the source, path, and site effects on strong ground motion during the 1989 Loma Prieta earthquake: a preliminary result on pervasive nonlinear site effects." Bull. Seism. Soc. Am., 81, 1859–1884.
- Cremonini, M. G., Christiano, P., and Bielak, J. (1988). "Implementation of effective seismic input for soil-structure interaction systems." *Earthquake Engrg. and Struct. Dyn.*, 16, 615–625.
- Darragh, R. B. and Shakal, A. F. (1991). "The site response of two rock and soil station pairs to strong and weak ground motion." *Bull. Seism. Soc. Am.*, 81, 1885–1899.
- Drucker, D. C. and Prager, W. (1952). "Soil mechanics and plastic analysis or limit design." Q. Appl. Math., 10, 157–164.
- Elgamal, A. W. (1991). "Shear hysteretic elasto-plastic earthquake response of soil systems." *Earthquake Eng. Struct. Dyn.*, 20, 371–387.
- Field, E. H., Johnson, P. A., Beresnev, I. A., and Zeng, Y. (1997). "Nonlinear ground-motion amplification by sediments during the 1994 Northridge earthquake." *Nature*, 390, 599–602.
- Finn, W. D. L., Martin, G. R., and Lee, M. K. W. (1978). "Comparison of dynamic analysis of saturated sand." In *Proc. of the ASCE Geotechnical Engineering Division of Specialty Conference on Earthquake Engineering and Soil Dynamics*, pages 472–491, Pasadena, California, June.
- Finn, W. D. L. (1991). "Geotechnical engineering aspects of microzonation." In *Proc.* 4th Int. Conf. on Seismic Zonation, volume 1, pages 199–259, Stanford, California.
- Hardin, B. O. and Drnevich, V. P. (1972). "Shear modulus and damping in soils: measurement and parameter effects." J. Soil Mech. Found. Div., ASCE, 8, 473–496.
- Iai, S., Kameoka, T., Matsunaga, Y., and Abiko, K. (1995). "Response of a dense sand deposit during 1993 kushiro-oki earthquake." Soils and Foundations, 35, 115–131.
- Idriss, I. M. and Seed, H. B. (1968). "Seismic response of horizontal soil layers." *J. Soil Mech. Found. Div.*, 94, 1003–1031.
- Jarpe, S. P., Cramer, C. H., Tucker, B. E., and Shakal, A. F. (1988). "A comparison of observations of ground response to weak and strong ground motion at Coalinga, California." Bull. Seism. Soc. Am., 78, 421–435.
- Joyner, W. B. and Chen, A. T. F. (1975). "Calculation of non-linear ground response in earthquakes." *Bull. Seism. Soc. Am.*, 65, 1315–1336.

- Joyner, W. B. (1975). "A method for calculating nonlinear seismic response in two-dimensions." Bull. Seism. Soc. Am., 65, 1337–1357.
- Lysmer, J. and Kuhlemeyer, R. L. (1969). "Finite dynamic model for infinite media." J. Eng. Mech. Div. ASCE, 95, 859–877.
- Marsh, J., Larkin, T. J., Haines, A. J., and Benites, R. A. (1995). "Comparison of linear and nonlinear seismic responses of two-dimensional alluvial basins." *Bull. Seism. Soc.* Am., 85, 874–889.
- O'Connell, D. R. H. (1999). "Replication of apparent nonlinear seismic response with linear wave propagation models." *Science*, 283, 2045–2050.
- Ortiz, M., Pinsky, P. M., and Taylor, R. L. (1983). "Operator split methods for the numerical solution of the elastoplastic dynamic problem." *Comp. Meth. Appl. Mech. Eng.*, 39, 137–157.
- Porcella, R. L. (1980). "A typical accelerograms recorded during recent earthquakes." Seismic Engineering Program Report. May-August:1980, Geological Survey Circular, 854-B, 1-7.
- Sato, K., Kokusho, T., Matsumoto, M., and Yamada, E. (1996). "Nonlinear seismic response and soil property during strong motion." Special Issue of Soils and Foundations, Japanese Geotechnical Society, pages 41–52.
- Satoh, T., Sato, T., and Kawase, H. (1995). "Nonlinear behavior of soil sediments identified by using borehole records observed at Ashigara valley, Japan." *Bull. Seism. Soc. Am.*, 85, 1821–1834.
- Schnabel, P., Seed, H. B., and Lysmer, J. (1972). "Modification of seismograph records for effects of local soil conditions." *Bull. Seism. Soc. Am.*, 62, 1649–1664.
- Seed, H. B. and Idriss, I. M. (1968). "Seismic response of horizontal soil layers." J. Soil Mech. Found. Div., ASCE, 94, 1003–1031.
- Seed, H. B. and Idriss, I. M. (1969). "The influence of soil conditions on ground motions during earthquakes." J. Soil Mech. Found. Div. ASCE, 94, 93–137.
- Simo, J. C. and Taylor, R. L. (1986). "A return mapping algorithm for plane stress elastoplasticity." *Int. J. Num. Math. Eng.*, 22, 649–670.
- Streeter, V. L., Wylie, E. R., and Richart, R. F. (1974). "Soil motion computations by characteristic method." J. Geotechn. Eng. Div., ASCE, 100, 247–263.

- Trifunac, M. D. and Todorovska, M. I. (1996). "Nonlinear soil response 1994 Northridge, California, earthquake." *J. Geotechnical Engrg.*, 122, 725–735.
- Trochanis, A. M., Bielak, J., and Christiano, P. (1991). "Three-dimensional nonlinear study of piles." *J. Geotechnical Engrg.*, 117, 429–439.
- Wen, K. L., Beresnev, I. A., and Yeh, Y. T. (1994). "Nonlinear soil amplification inferred from downhole strong seismic motion data." *Geophys. res. Lett.*, 21, 2625–2628.
- Xu, J. (1998). "Three-dimensional simulation of wave propagation in inelastic media on parallel computers." *Ph.D Thesis*, Carnegie Mellon University, Pittsburgh, PA.
- Yu, W., Anderson, J. G., and Siddharthan, R. (1993). "On the characteristic of nonlinear soil response." *Bull. Seism. Soc. Am.*, 83, 218–224.
- Zhang, B. and Papageorgiou, A. S. (1996). "Simulation of the response of the marina district basin, san francisco, california, to the 1989 loma prieta earthquake." *Bull. Seism. Soc. Am.*, 86, 1382–1400.